Accepted Manuscript

The effect of cation disorder on magnetic properties of new double perovskites $La_2Ni_xCo_{1-x}MnO_6$ (x = 0.2 - 0.8)

A. Harbi, H. Moutaabbid, Y. Li, Carlos Renero-Lecuna, M. Fialin, Y. Le Godec, S. Benmokhtar, M. Moutaabbid

PII: S0925-8388(18)34059-3

DOI: https://doi.org/10.1016/j.jallcom.2018.10.360

Reference: JALCOM 48178

To appear in: *Journal of Alloys and Compounds*

Received Date: 22 May 2018

Revised Date: 22 October 2018

Accepted Date: 27 October 2018

Please cite this article as: A. Harbi, H. Moutaabbid, Y. Li, C. Renero-Lecuna, M. Fialin, Y. Le Godec, S. Benmokhtar, M. Moutaabbid, The effect of cation disorder on magnetic properties of new double perovskites $La_2Ni_xCo_{1-x}MnO_6$ (x = 0.2 - 0.8), *Journal of Alloys and Compounds* (2018), doi: https://doi.org/10.1016/j.jallcom.2018.10.360.

The effect of cation disorder on magnetic properties of new double perovskites $La_2Ni_xCo_{1-x}MnO_6$ (x = 0.2 - 0.8)

A. Harbi[1], H. Moutaabbid[2], Y. Li[3], Carlos Renero-Lecuna[4], M. Fialin[5], Y. Le Godec[2], S. Benmokhtar[1], M. Moutaabbid[1]

[1] University of Casablanca, Laboratory of Chemistry and Physics of Materials LCPM, Faculty of Sciences, Department of Chemistry, Casablanca, Morocco.

[2]Institut de Minéralogie et de Physique des Matériaux et Cosmochimie, Sorbonne Université, 4 place Jussieu 75005 Paris, France.

[3]Institut Parisien de Chimie Moléculaire, Sorbonne Universités, CNRS UMR 8232, 4 place Jussieu, Paris 75252, France.

[4]Grupo de Nanomedicina - IDIVAL, Facultad de Medicina, Universidad de Cantabria, Avd. Cardenal Herrera Oria s/n, 39011 Santander, Spain.

[5]Service Camparis, UMR7154 - CNRS, Institut de Physique du Globe, Paris.

Cation disorder in new double perovskites $La_2Ni_{1-x}Co_xMnO_6$

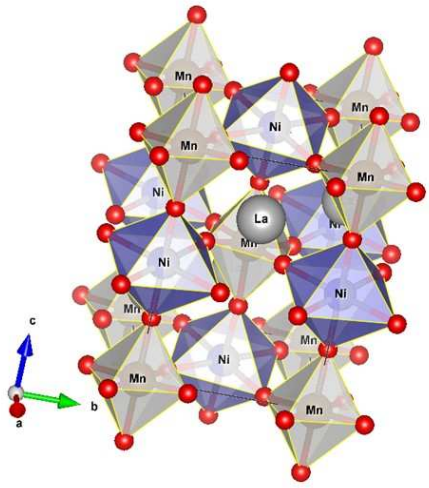

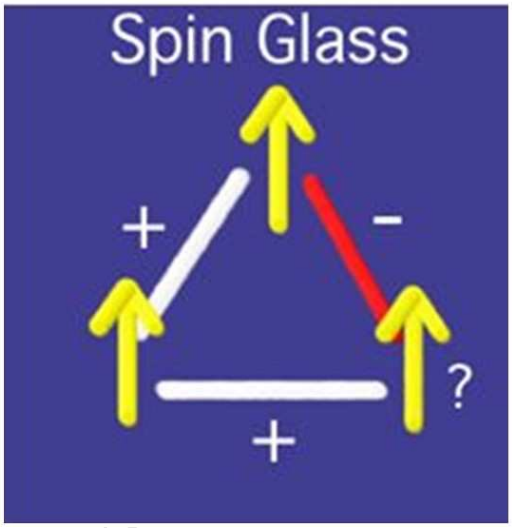

1. Introduction

Double Perovskite-type oxides of general chemical formula $A_2BB'O_6$, (where A = alkaline earth or rare-earth ion), the transition metal sites are alternately occupied by two different types of cations B and B'. It is clear that both the valence and the ionic size of B and B' are crucial in affecting the physical properties of the systems. They have been studied extensively not only due to the versatile nature of their structure but more importantly due to their multifunctional properties [1]. Among recent research a wide range of ground states appear, including ferromagnetic metals, orbital- and charge-ordered antiferromagnets, and more complex stripe and spin-glass states [2]. Simple perovskites $Pr_{0.5}Ca_{0.5-x}Sr_xMnO_3$ [3] $La_{0.67}Ca_{0.33}Mn_{0.9}Fe_{0.1}O_3$ [4] exhibits this spin glass behavior but also double perovskite $A_2B'B''O_6$ compounds that appear to be spin-glasses, or spin-glass like behavior. For example, spin-glass behavior has been found in the disordered $Sr_2FeB'O_6$ compounds with B'= Nb, Ta or Ru [1]. The spin-glass behavior likely arises from a competition between ferromagnetic and antiferromagnetic interactions because of local disorder such as in particular La_2CoMnO_6.

Double-perovskite La_2NiMnO_6 is a single material platform with multiple functions and is expected to have unprecedented device applications [5], it has received considerable attention recently because the material has a relatively high Curie temperature (*Tc*) of 280 K [6] and a colossal magneto dielectric coupling (up to ~20%) over a wide temperature range across room temperature [5,7]. A giant tunability of dielectric permittivity was also reported [8]. La_2NiMnO_6 is a ferromagnetic insulator with a positive super-exchange interaction between Ni and Mn cations [5, 6, 9-12]. Such behavior is significant in spintronic materials as it helps to achieve magneto- dielectric properties. These outstanding physical properties arise from competing magnetic interactions of cations, structural (phonons) and polarization (charges) order parameters.

La_2CoMnO_6 shows well-ordered monoclinic symmetry with good ferromagnetic and insulating behaviors [12-13]. Using first principle density functional calculations, it is stated that the insulating state in La_2CoMnO_6 is driven by the Coulomb-assisted spin-orbit coupling operative within the Co-d manifold [14]. La_2CoMnO_6 shows two ferromagnetic transitions at T_{C1} ~ 225 K and T_{C2} ~ 150K [14]. Blasse et al. showed the presence of ferromagnetic Co^{2+}–

Mn^{4+} superexchange interaction [15]. Joy et al. presented the high-spin Mn^{3+} and low-spin Co^{3+} in rhombohedral phase and high spin Co^{2+} and Mn^{4+} in orthorhombic phase in La_2CoMnO_6 [16]. By performing X-ray absorption near-edge spectroscopy (XANES) experiments Joly et *al*. also suggested that the order phase involves Co^{2+} and Mn^{4+} ions and disorder state corresponds to Co^{3+} and Mn^{3+} ions in $LaCo_{0.5}Mn_{0.5}O_3$ [17].

In the present work, the double perovskites $La_2Ni_xCo_{1-x}MnO_6$ (LNCMO) with x = 0.2, 0.25, 0.5, 0.75 and 0.8 have been prepared by new solid-state reaction. The powder XRD, IR, UV and Raman spectroscopy at room temperature, has done the structural characterization. The magnetic properties have been investigated by ZFC-FC and AC magnetic measurements from 2 K to 300 K and the optical properties have been investigated in order to calculate the band gap energy and to study the optical behavior of the samples.

2. Sample preparation

Polycrystalline samples of $La_2Ni_xCo_{1-x}MnO_6$ (x = 0.2, 0.25, 0.5, 0.75, 0.8) were synthesized by solid-state reaction. Stoichiometric amounts of La_2O_3 (99%), $CoCO_3$ (98%), NiO (99%) and $MnCO_3$ (99%) were mixed and heated in air at 200°C for 6 h, 500°C for 6 h and finally at 900ºC for 24 h in a conventional tubular furnace. After the first step, the material was re-grounded in an agate mortar, which were subsequently heated at 1000 ºC for 24h in air. The $La_2Ni_xCo_{1-x}MnO_6$ compounds were synthesized at the same temperatures.

The chemical reaction is :

$$La_2O_3 + x\ NiO + (1-x)\ CoCO_3 + MnCO_3 \rightarrow La_2Ni_xCo_{1-x}MnO_6 + (1+x)\ CO_2 \uparrow$$

The structural refinements were undertaken from the powder data. Diffraction data were collected at room temperature on a Phillips D 5000 (θ–θ) diffractometer: Bragg–Brentano geometry; diffracted-beam graphite monochromator; Cu(K_α) radiation (40 kV, 40 mA); Soller slits of 0.02 rad on incident and diffracted beams; divergence slit of 0.5º; antiscatter slit of 1º; receiving slit of 0.1 mm; with sample spinner. The patterns were scanned through steps of 0.02 (2θ), between 10 and 100 (2θ) with a fixed-time counting. The full pattern refinements were carried out by means of the Rietveld method using the Fullprof program [18] integrated in Winplotr software [19]. The Rietveld refinement of the observed powder XRD data is initiated with scale and background parameters and successively other profile parameters are included. The background is fitted with a fifth order polynomial. The peak shape is fitted with a pseudo-Voigt profile function. After an appreciable profile

matching the position parameters and isotropic atomic displacement parameters of individual atoms were also refined.

The chemical composition and purity of each sample was recorded using Cameca SX100 electron microprobe at the CAMPARIS facility (Sorbonne University).

Fourier transform infrared spectroscopy (FT-IR, NICOLET 6700) was used to determine chemical bonding of powders.

The Raman spectra were recorded on HR460 (Jobin-Yvon/Horiba) spectrometer using as excitation source an Ar^+ laser under 514.5 nm excitation wavelength.

The optical properties UV-visible spectroscopy measurements was done using Perkin Elmer UV-VIS spectrometer (Lambda 1050).

The All direct current (DC) and alternative current (AC) magnetization measurements have been carried out on a Quantum Design MPMS-XL7 magnetometer.

3. Results and discussion

3.1. Structural characterization

The Rietveld refinement of X-ray diffraction patterns of the polycrystalline $La_2Ni_xCo_{1-x}MnO_6$ (x = 0.2, 0.25, 0.5, 0.75, 0.8) confirmed the presence of a majority monoclinic structure phase with $P2_1/n$ space group and a small minority phase marked by (☆) sign was estimated to be around 6.08% for x = 0.2, 6.14% for x = 0.25, 5.6% for x = 0.5, 7.31% for x = 0.75, 6.76% for x = 0.8) of La_2MO_4 with M = Ni, Co, Mn (orthorhombic, Bbam space group, with a=5.4652 Å, b=5.46869 Å, c=12.67804 Å) previously reported in [20]. The lattice parameters and volume obtained from refinement using monoclinic $P2_1/n$ space group are found similar to the reported values of monoclinic La_2CoMnO_6 double perovskite [21]. After the complete refinement, we achieved a good agreement between the observed and calculated XRD patterns at 298K, for $La_2Ni_xCo_{1-x}MnO_6$ (x = 0.2, 0.25, 0.5, 0.75, 0.8) as shown in Figure 1, respectively as a representative of the series. Table 1 summarizes the lattice parameter, unit cell volume and reliability factors after the Rietveld refinement, one note a strange anomaly of decreasing unit volume with increasing x shown at x = 0.75, probably attributed to the presence of La_2MO_4. The selected bond lengths were determined and are listed in Table 2. The results of Rietveld refinements data showing that the atoms (Ni/Co) and Mn are octahedrally coordinated with the oxygen atoms. The octahedra [Ni/CoO_6] and [MnO_6] are linked by O_1 and O_3 along (a, b) axis and by O_2 along c-axis in Figure 2.

3.2. The electron probe microanalysis results

The elementary analysis has been performed by electron Probe Microanalysis in Tables 3, the average stoichiometry of our double perovskite samples can be written as $La_{2.05}Ni_{0.21}Co_{0.76}Mn_{0,96}O_{6\pm\delta}$, $La_{2.6}Ni_{0.34}Co_{0.72}Mn_{1.1}O_{6\pm\delta}$, $La_{1.9}Ni_{0.57}Co_{0.48}Mn_{0.93}O_{6\pm\delta}$, $La_{2.07}Ni_{0.77}Co_{0.18}Mn_{0.96}O_{6\pm\delta}$, and $La_{2,05}Ni_{0.83}Co_{0,25}Mn_{1.08}O_{6\pm\delta}$ The disagreement with the theoretical stoichiometry, can be justified by the presence of the impurity phase of La_2MO_4 with M = Ni, Co, Mn.

3.3. Raman spectroscopy studies

Figure 3 shows the Raman spectra of the studied compounds. The main features of these spectra are two broad peaks at around 520 cm^{-1} and 650 cm^{-1}. According to the bibliography [22-25] these bands corresponds to the Ni/Co–O and Mn-O octahedron antisymmetric (B_g) and symmetric (A_g) stretching vibrations respectively, for a monoclinic $P2_1/n$ crystal. The energy of the phonons and the values of the FWHM for each sample are summarized in Table 4. We observed a hardening in both phonons as the amount of Ni^{2+} doping increase. Despite the fact that the ionic radii of the Co^{+2} and Ni^{2+} in octahedral sites are 0.65 Å and 0.69 Å respectively [26] and the average of the distances Co/Ni-O, Mn-O, the octahedron La-O are maintained the same for the different Nickel contents (Table 2). The hardening of the phonons can be associated to a general relaxation of the host lattice, when Ni^{2+} is incorporated to the lattice Figure 4. The opposite occurs in the case of the double perovskites La_2NiMnO_6 and La_2CoMnO_6 when doped with Ca^{+2} ions. The hypothesis of this lattice relaxation gets stronger since the observed FWHM does not change with the doping increase Figure 5.

3.4. Infrared spectroscopy studies.

Figure 6 shows FT-IR spectra of the studied compounds. The broad absorption band at about 426 cm^{-1} and 600 cm^{-1} can be assigned to the Ni/Co–O and Mn-O bond stretching vibration and deformation modes of the [Ni/CoO_6] and [MnO_6] octahedra according to the literature [27-28].

3.5. The optical studies.

The energy band gap of $La_2Ni_xCo_{1-x}MnO_6$ (x = 0.2, 0.25, 0.75, 0,8) were studied by optical absorption. The band gap of samples was calculated by plotting graph between $(\alpha h\upsilon)^2$ against the photon energy hυ, with help of optical absorbance where α is the absorption coefficient, h is the Plank constant and υ is the frequency of incident light. Tauc's relation is given by [29]:

$Ah\upsilon = A\,(h\upsilon - E_g)^n$

Where E_g is the energy difference between valence and conduction band and n is a constant equal to 1/2 for direct band gap materials and 2 for indirect band gap material. The natures of the plots indicate the existence of direct transitions. The band gap E_g is determined by extrapolation of the straight portion of the plot to the energy axis as shown in Figure 7. The obtained band gap of $La_2Ni_xCo_{1-x}MnO_6$ (x = 0.2, 0.25, 0.75, 0.8) is given in Table 5.

3.6. The magnetic properties studies

Figure 8 summarizes the results obtained from ZFC-FC magnetization in a field of 50 Oe between 2 K and 300 K : (a) shows the thermal variation of molar susceptibilities or susceptibility per formula unit (f.u.) for the five double perovskites; (b), the enlarged ZFC χ_M curves in the temperature range of 2 - 300 K ; (c), the derivatives of ZFC χ_M against T (dM/dT) between 180 K and 300 K (the solid lines are eye guides) and (d), the inverted ZFC molar susceptibility, χ_M^{-1}, against T between 220 K and 300 K (the solid lines represent the data fitted by Curie-Weiss law). All five oxides present a strong paramagnetic (PM) to ferromagnetic (FM) transition with the Curie temperature, T_{C1}, corresponding to the deepest minimum value of $d\chi_M/dT$.

The T_{C1} value increases from 232 K to 260 K (see Table 6) when x increases from 0.2 to 0.8.This is expected, as the T_{C1} value of LNMO oxide reported in the literature are very near room temperature : for example, 270 K for a polycrystalline sample [31] and thin film [32], 284 K for large nanoparticles (d>50 nm) [33] and 288 K for a single crystal [34]. Whereas T_{C1} value of pure LCMO oxides are lower and ranges from 210 K to 235 K for polycrystalline samples [35-38] and thin films [39,42]. Obviously, T_{C1} depends not only on the oxide composition but also on its cation orderings. The strong PM-FM transition in double perovskites is attributed to the long-range magnetic ordering of Mn^{4+}- O - M^{2+} (M^{2+} = Co or Ni or other transition metals) [43], which is always in competition with the antiferromagnetic interactions (AFM) of anti-site ions (Mn^{4+} - O - Mn^{4+} or B^{2+} - O - B^{2+}). The later ones are the consequences of the local disorders in double perovskites, such as oxygen vacancy [43,40], B-site disordering [32, 36] which reduces the long-range FM ordering of Mn^{4+} - O - B^{2+}. Even in an ordered LBMO perovskite, the antiphase interface between the two FM regions would have also AFM interactions of antisite ions. Therefore, for a double perovskite of a given composition, a higher T_{C1} reflects a higher degree of cation ordering. Three of the fives double perovskites with (x = 0.2, 0.25, 0.5) content show also a weak PM-FM transition at T_{C2}

= 200 K, 200K and 208K respectively. The similar transition occurs often in LNMO oxides and is attributed to the short-range magnetic ordering of Mn^{4+}- O - Ni^{2+} [32, 34, 31]. All values of T_{C1} and T_{C2} are summarized in the Table 6 together with the Curie-Weiss parameters, C and Θ. The positive sign of Θ confirms the ferromagnetic ground state in the fives double perovskites. T_{C1} and Θ show the same tendency of compositional variation and the small difference between them suggests a high degree of cation ordering in double perovskite [44].

It's worth noting that in a certain temperature domain above T_{C1}, χ_M^{-1} versus T (Figure 8 d) presents an upward deviation from Curie-Weiss behavior, as already observed for a polycrystalline LNMO [45] and a nanoparticle LNMO [46] by S.M. Zhou et al. They explained the phenomenon by the existence of a short-range FM ordered state persisting above T_{C1}.

The Figure 9 shows the *M-H* loops of the fives double perovskites at 5 K: (a) presents the entire M-H loops from -7 *T* to 7 *T* and (b), the zoomed loops from -2*T* to 2*T* without first magnetizations. Each hysteresis *M-H* loop is characterized by its specific magnetization at 7 *T* (M_S), its coercive magnetic field (H_C) and by its specific remnant magnetization (M_r), and the Table 7 summarizes the values of these parameters. For the LCMO and LNMO doubles perovskites these three parameters depend strongly on the content of the antisite ions and of anti-phases. If the disorder increases, both M_S and M_r diminish, whereas H_C decreases [43,33]. When the M_S of a double perovskite approaches its theoretical spin-only value ($M_{S.LCMO}$ = 6.0 μ_B/f.u. and $M_{S.LNMO}$= 5.0 μ_B/f.u.), the oxide is considered as well ordered. For example, A J Baron-Gonzalez *et al* has studied the effect of cation disorder on the structural, magnetic and dielectric properties of two polycrystalline La_2CoMnO_6 double perovskite with the disorder degree of 95% and 74% respectively [35], the highly ordered LCMO (T_{C1} = 235 K) has a M_S value of 5.85 μ_B/f.u. and a H_C value of 1.50 kOe at 10 K, whereas the lowly ordered LCMO (T_{C1} = 225 K), a M_S value of 4.41 μ_B/f.u. and a H_C value of 6.75 kOe; M.P. Singh *et al* has compared the structural, magnetic and optic properties of two LNMO thin films: an ordered La_2NiMnO_6 film (T_{C1} = 270 K) and its disordered $LaNi_{0.5}Mn_{0.5}O_3$ counterpart (T_{C1} = 138 K). The M_S and H_C are respectively 4.8 μ_B/f.u. 0.25 kOe for the former, and 3.7 μ_B/f.u. and 1 kOe for the second [32].

The spin-only saturation magnetization of our double perovskites, M_{S0}, can be calculated by the following equation:

$$M_{S0} = \sqrt{(1-x)\, M_{S.LCMO}^2 + x\, M_{S.LNMO}^2}$$

The ratio of M_S/M_{S0} allows an estimation of the ordering degree for the five double perovskites (see the Table 7). According to this criterion, the Ni^{2+} rich double perovskites (x = 0.75 and 0.80) have a high degree of ordering (> 96%), while the oxide with x = 0.25, the lowest degree of cation ordering. As expected the H_c value tend to decrease with Ni^{2+} content in the oxides.

The *M-H* loops curves at 300 K have no hysteresis opening. The Figure 10 shows *M-H* curves from 0 to 7 *T* for the five double perovskites. In low field (< 2 T) the *M* plotted against *H* are straight lines, but in high field (> 2 *T*) one observes a notable downward deviation of *M* from the straight lines for all the fives oxides. This confirms the existence of the short-range ordering above T_{C1} mentioned above. More is the Ni^{2+}content in the oxides, more is the downward deviation of their *M-H* curves.

The Figure 11 (a) and (j) illustrates the thermal variation of the in-phase (χ') and out-off phase (χ'') components of *ac* molar susceptibilities for the five double perovskites under an *ac* field of 3 Oe at three frequencies (50.0 Hz, 141.6 Hz and 400.6 Hz). Both χ' and χ'' display frequency dependence in the whole temperature range of 15 – 300 K: their intensities decrease with increasing frequency. The χ'-*T* curves are very similar to the ZFC χ_M-*T* curve, indicating two PM-FM transitions of the three oxides with x = 0.20, x = 0.25 and x = 0.50, and one transition for the two others rich in Ni^{2+} with x = 0.75 and x = 0.80. The χ''-T curves give more information on the multiple magnetic transitions in the oxides: they revealed that the positions of the strong and weak PM-FM transitions at T_{C1ac} and T_{C2ac} are frequency independent, whereas the transition below 100 K (T_{f1} at 50 Hz , T_{f2} at 141.6 Hz and T_{f3} at 400.6 Hz) are strongly frequency dependent. Furthermore, one can observe that the peak relative to the weak PM-FM transition is very large in the χ''-*T* curve for the double perovskite having x = 0.25, it seems that the broadening of this peak might result from the addition of several short-range FM interactions of magnetic cations. This is consistent with the fact this oxide has the lowest ordering degree (Table 7) and suggests that it might have a less homogeneous structure. The Table 8 lists the values of T_{C1ac}, T_{C2ac}, T_{f1}, T_{f2} and T_{f3} for the five double perovskites.

The low temperature frequency dependent anomaly has been already observed in several LCMO and LNMO double perovskites, and is generally assigned to the spin or cluster glass transition. The spin glass behavior results from the competition between FM and

AFM interactions in many magnetic oxides, which destroys the long-range magnetic order and leaves the system in a random spin configuration of frozen state. If one FM or AFM interaction dominates, the FM-AFM competition is weak; the system will have a short magnetic order, and thus a cluster glass behavior. The spin or cluster glass is characterized by their specific relaxation time τ_0 as well as by their frequency sensitivity factors, called also Mydosh factor $K = \Delta T_f / (T_{f0}\, \Delta(\log_{10} f))$ [47,48].

The relaxation time τ_0 can be derived from Arrhenius law.

$$\tau = \tau_0 \exp[E_a /(k_B T_f)]$$

Where E_a is the anisotropy energy, $\tau=1/(2\pi f)$ and k_B, the Boltzmann constant.

The Table 9 summarizes the τ_0 and K values calculated from χ''-T curves for the fives double perovskites. The τ_0 value of the five oxides varies from 1.963×10^{-10} to 2.974×10^{-7} s and is greater than the τ_0 value of spin glass (about 10^{-13} s). This reveals the cluster glass nature of the low temperature frequency dependent anomalies on the χ''-T curves. The K values greater than 0.1 indicate that the magnetic clusters are non-interacting superparamagnetic single domains.

Conclusion

In conclusion, we succeed in the new solid-state synthesis of five doubles perovskites oxide $La_2Ni_xCo_{1-x}MnO_6$ (x = 0.2, 0.25, 0.5, 0.75, 0.8). Raman and IR spectra show strong bands respectively at (650, 520 cm^{-1}) and (426, 600 cm^{-1}), attributed to the stretching vibration of Ni/Co–O and Mn–O bonds in the structure. UV exhibits semiconductor behaviors for all samples. We have done a preliminary magnetic characterization of the method by ZFC-FC M-T in a weak field, by hysteresis M-H loops at 5 K and 300 K and by *ac* magnetizations between at three frequencies. The double perovskites having $x \leq 0.5$ show two PM-FM transitions and ones with $x \geq 0.75$, only one PM-FM transition. As expected the Curie temperature of the strong PM-FM transition (T_{C1}) increases with increasing content of Ni^{2+}. All the five monoclinic structure ($P2_1/n$ space group) double perovskites display a superparamagnetic behavior below 100K.

[1] S. Vasala, M. Karppinen, $A_2B'B''O_6$ perovskites A review, J. Prog. Solid. State. Chem 43 (2015) 1-36. https://doi.org/10.1016/j.progsolidstchem.2014.08.001

[2] M. B. Salamon, M. Jaime, The physics of manganites: Structure and transport ,J. Rev. Mod. Phys. 73, (2001) 583 – 628. https://doi.org/10.1103/RevModPhys.73.583

[3] S. Krupicka, M. Marysko, Z. Jirak, J. Hejtmanek, Details of structural and magnetic transitions in Pr0.5Ca0.5−xSrxMnO3 perovskites, J. Magn. Magn. Mater 206 (1999) 45-67. https://doi.org/10.1016/S0304-8853(99)00496-5

[4] Jian-Wang Cai, Cong Wang, Bao-Gen Shen, Jian-Gao Zhao,Wen-Shan Zhan. ,Colossal magnetoresistance of spin-glass perovskite $La_{0.67}Ca_{0.33}Mn_{0.9}Fe_{0.1}O_3$, Appl. Phys. Lett. 71 12, (1997) 1727-1729. https://doi.org/10.1063/1.120017

[5] R.I. Dass, J.Q. Yan, J.B. Goodenough, Oxygen stoichiometry, ferromagnetism, and transport properties of La2−xNiMnO6+δ, Phys. Rev. B 68 (2003) 064415 1-12. https://doi.org/10.1103/PhysRevB.68.064415

[6] N.S. Rogado, J. Li, A.W. Sleight, M.A. Subramanian, Magnetocapacitance and Magnetoresistance Near Room Temperature in a Ferromagnetic Semiconductor: La_2NiMnO_6,J. Adv. Mater. 17 (2005) 2225-2227. https://doi.org/10.1002/adma.200500737

[7] D. Choudhury, P. Mal, R. Mathieu, A. Hazarika, S. Rajan, A. Sundaresan, U.V. Waghmare, R. Knut, O. Karis, P. Nordblad, D.D. Sarma, Near room-temperature colossal magnetodielectricity and multiglass properties in partially-disordered La_2NiMnO_6, Phys. Rev.B. 108 (2012) 127201 1-5. https://doi.org/10.1103/PhysRevLett.108.127201.

[8] M.H. Tang, J.W. Hou, J. Zhang, G.J. Dong, W. Shu, The giant dielectric tunability effect in bulk La_2NiMnO_6 around room temperature, J. Solid. State. Commun. 150 (2010) 1453-1456. https://doi.org/10.1016/j.ssc.2010.05.029

[9] J. B. Goodenough, A. Wold, R. J. Arnott, N. Menyuk, Relationship Between Crystal Symmetry and Magnetic Properties of Ionic Compounds Containing Mn^{3+}, J. Phy. Rev.124 (1961) 373-384.https://doi.org/10.1103/PhysRev.124.373

[10] Mao, Yuanbing, Jason Parsons, John S. McCloy, Magnetic properties of double perovskite La_2BMnO_6 (B = Ni or Co) nanoparticles, J. Nanoscale 5 (2013) 4720-4728. https://doi.org/10.1039/C3NR00825H

[11] V. L. Joseph Joly, P. A. Joy, S. K. Date, Two ferromagnetic phases with different spin states of Mn and Ni in $LaMn_{0.5}Ni_{0.5}O_3$, Phy. Rev.B 65 (2002) 184416 1-12. https://doi.org/10.1103/PhysRevB.65.184416

[12] R. I. Dass, J. Q. Yan, J. B. Goodenough, Multiple magnetic phases of $La_2CoMnO_{6-\delta}$ ($0<\sim\delta<\sim0.05$),Phys. Rev.B 67 (2003) 014401 1-9 .https://doi.org/10.1103/PhysRevB.67.014401

[13] M. P. Singh, S.Charpentier, K. D.Truong, P.Fournier, Evidence of bidomain structure in double-perovskite La_2CoMnO_6 thin films, Appl. Phys. Lett.90 (2007) 211915 1-3. https://doi.org/10.1063/1.2743387

[14] S. Baidya, T. Saha-Dasgupta, Electronic structure and phonons in La_2CoMnO_6: A ferromagnetic insulator driven by Coulomb-assisted spin-orbit coupling, Phys. Rev.B 84 (2011) 035131 1-4. https://doi.org/10.1103/PhysRevB.84.035131

[15] G. Blasse, Ferromagnetic interactions in non-metallic perovskites, J. Phys. Chem. Solids 26 (1965) 1969-1971. https://doi.org/10.1016/0022-3697(65)90231-3

[16] P. A. Joy, Y. B. Khollam, S. K. Date, Spin states of Mn and Co in $LaMn_{0.5}Co_{0.5}O_3$, Phys. Rev.B 62 (2000) 8608-8610. https://doi.org/10.1103/PhysRevB.62.8608

[17] V. L. Joseph Joly, Y. B. Khollam, P. A. Joy, C. S. Gopinath, S. K. Date, The origin of ferromagnetism in the two different phases of $LaMn_{0.5}Co_{0.5}O_3$: evidence from x-ray photoelectron spectroscopic studies, J. Phys. Condens. Matter 13 (2001) 649–656. https://doi.10.1088/0953-8984/13/4/311

[18] J. Rodriguez-Carvajal, Recent advances in magnetic structure determination by neutron powder diffraction, J. Physica B 192 (1993) 55-69. https://doi.org/10.1016/0921-4526(93)90108-I

[19] T. Roisnel, J. Rodriguez-Carvajal, WinPLOTR: A Windows Tool for Powder Diffraction Pattern Analysis, Mater. Sci. Forum 378-381 (2001) 118-123. https://doi.org/10.4028/www.scientific.net/MSF.378-381.118

[20] G. Pecchi, R. Morales, D. Salinas, Eduardo J. Delgado, J. Luis García Fierro, Catalytic Performance of $La_{0.6}Ca_{0.4}Fe_{1-x}Ni_xO_3$ Perovskites in DME Oxidation, J. Mod Res Cat, 4 (2015) 97-106. https://doi.org/10.4236/mrc.2015.44012

[21] B. Orayech, I. Urcelay-Olabarria, G. A. López, O. Fabelo, A. Faike, J. M. Igartuac, Synthesis, structural, magnetic and phase-transition studies of the ferromagnetic La_2CoMnO_6 double perovskite by symmetry-adapted modes, J. RSC. 44 (2015) 13867 –13880. https://doi.org/10.1039/C5DT01532D

[22] Guo, Yuqiao, Lei Shi, Shiming Zhou, Jiyin Zhao,Shiqiang Wei.Supercond, Local Valence and Hole-Doping Effect on Magnetic Properties in Double Perovskite La_2NiMnO_6, J. Nov Magn. 26 (2013) 3287–3292. https://doi.org/10.1007/s10948-013-2168-6

[23] M. N. Iliev, H. Guo, A. Gupta, Raman spectroscopy evidence of strong spin-phonon coupling in epitaxial thin films of the double perovskite La_2NiMnO_6, Appl. Phys. Lett 90 (2007) 151914 1-3. https://doi.org/10.1063/1.2721142

[24] Dhirendra Kumar, V. G.Sathe, Raman spectroscopic study of structural transformation in ordered double perovskites La_2CoMnO_6 bulk and epitaxial film,J .Solid. State. Commun 224 (2015) 10-14. https://doi.org/10.1016/j.ssc.2015.09.014

[25] El-Kemary, M., N. Nagy, and I. El-Mehasseb, Fabrication and characterization of semiconductor nickel oxide (NiO) nanoparticles manufactured using a facile thermal treatment J. Mater. Sci. Semicond. Process 16 (2013) 1747–1752. https://doi.org/10.1016/j.rinp.2016.11.031

[26] R. D. Shannon, Revised effective ionic radii and systematic studies of interatomic distances in halides and chalcogenides, *Acta Cryst A*, 32 5 (1976) 751–767. https://doi.org/10.1107/S0567739476001551

[27] Li, Changnian, Bangxu Liu, Yanyan He, Chao Lv, Hua He, Yebin Xu, Preparation, characterization and dielectric tunability of La_2NiMnO_6 ceramics, J. Alloys. Compd 590 (2014) 541-545. http://dx.doi.org/10.1016/j.jallcom.2013.12.170

[28] G. V. Subba Rao and C. N. R. Rao, Infrared and Electronic Spectra of Rare Earth Perovskites: Ortho-Chromites, -Manganites and –Ferrites, J. Appl. Spectrosc 24 (1970) 436-445. https://doi.org/10.1366/000370270774371426

[29] Chang, Hong, Yu Gao, Fang Liu, et al, Effect of synthesis on structure, oxygen voids, valence bands, forbidden band gap and magnetic domain configuration of La_2CoMnO_6 ,J. Alloys. Compd 690 (2017) 8-14. https://doi.org/10.1016/j.jallcom.2016.08.086

[30] Lan, Chunfeng, Shuai Zhao, Tingting Xu, et al, Investigation on structures, band gaps, and electronic structures of lead free La_2NiMnO_6 double perovskite materials for potential application of solar cell, J. Alloys.Compd 655 (2016) 208-214. https://doi.org/10.1016/j.jallcom.2015.09.187

[31] Qiu-hang Li, Na Li , Jian-zhong Hu , Qi Han , Qing-shan Ma , Lei Ge , Biao Xiao , and Ming-xiang Xu, The effect of Ca-substitution in La-site on the magnetic properties of La_2CoMnO_6, J. Appl. Phys. 116 (2014) 033905 1-5. https://doi.org/10.1063/1.4890321

[32] S. M. Zhou, Y. Q. Guo, J. Y. Zhao, S. Y. Zhao, L. Shi. Nature of short-range ferromagnetic ordered state above T_C in double perovskite La2NiMnO6, Appl. Phys. Lett. 96 (2010) 262507 1-4. https://doi.org/10.1063/1.3459141

[33] M. P. Singh, K. D. Truong, S. Jandl, P. Fournier. Long-range Ni/Mn structural order in epitaxial double perovskite La_2NiMnO_6 thin films, Phys. Rev. B, 79 (2009) 224421 1-3. https://doi.org/10.1063/1.3360352

[34] S. Zhao, L. Shi, S. Zhou, J. Zhao, H. Yang Y. Guo. Size-dependent magnetic properties and Raman spectra of La2NiMnO6 nanoparticles, J. Appl. Phys, 106 (2009) 123901 1-5. https://doi.org/10.1063/1.3269707

[35] J. B.Gonzalez, C. Frontera, J. L. G.Munoz, B. R.Murias, J .Blasco, Effect of cation disorder on structural, magnetic and dielectric properties of La_2MnCoO_6 double perovskite, J. Phys. Condens. Matter, 23 (2011) 496003 1-5. https://doi.org/10.1088/0953-8984/23/49/496003

[36] K. Devi Chandrasekhar, A. K. Das, A. Venimadhav, Synthesis and Magnetic Properties of La2NiMnO6 Nanoparticles, AIP Conference Proceedings 1347 (2011) 23-26. https://doi: 10.1063/1.3601778

[37] R. Egoavil, S. Hühn, M. Jungbauer, N. Gauquelin, A. Béché, G. Van TendelooVerbeecka, V. Moshnyaga, Phase problem in the B-site ordering of La_2CoMnO_6: impact on structure and magnetism, J. Nanoscale,7 (2015) 9835-9843. https://doi.org/10.1039/c5nr01642h

[38] Lei Xing, Qiuhang Li and Mingxiang Xu. Magnetic properties and magnetoresistance effect of $La_2Co_{1-x}Mg_xMnO_6$ ($0.1 \leq x \leq 1.0$), J. Mater. Res. Express 4 (2017) 046102 1-14. https://doi.org/10.1088/2053-1591/aa6920

[39] H. Z. Guo, A. Gupta, T. G. Calvarese, M. A. Subramanian, Structural and magnetic properties of epitaxial thin films of the ordered double perovskite La_2CoMnO_6, Appl. Phys. Lett.89 (2006) 262503 1-9. https://doi.org/10.1063/1.2422878

[40] M. N. Iliev, M. M. Gospodinov, M. P. Singh, J. Meen, K. D. Truong, P. Fournier, S. Jandl . Growth, magnetic properties, and Raman scattering of La_2NiMnO_6 single crystals, J. Appl. Phys, 106 (2009) 023515 1-4. https://doi.org/10.1063/1.3176945

[41] P. Kumar, S. Ghara, B. Rajeswaran, D.V.S. Muthu, A. Sundaresan, A. K. Sood, Temperature dependent magnetic, dielectric and Raman studies of partially disordered. La_2NiMnO_6, J. Solid. State. Commun. 184 (2014) 47–51 https://doi.org/10.1002/adma.200500737

[42] M. K. Kim, J. Y. Moon, H. Y. Choi, S. H. Oh, N. Lee, Y. J. Choi, Effects of different annealing atmospheres on magnetic properties in La_2CoMnO_6 single crystals, J. Current Appl Phys 15 (2015) 776 – 779. https://doi.org/10.1016/j.cap.2015.04.009

[43] R. I. Dass, J. B. Goodenough, Multiple magnetic phases of $La_2CoMnO_{6-\delta}$ ($0 \leq \delta \leq 0.05$), Phys. Rev.B. 67 (2003) 014401 1-4. https://doi.org/10.1103/PhysRevB.67.014401

[44] M. Balli, P. Fournier, S. Jandl ,M. M. Gospodinov, A study of the phase transition and magnetocaloric effect in multiferroic La_2MnNiO_6 single crystals, J. Appl. Phys. 115 (2014) 173904 1-8. https://doi.org/10.1063/1.4874943

[45] H. Z. Guo, A. Gupta, J. Zhang, M. Varela, S. J. Pennycook, Effect of oxygen concentration on the magnetic properties of La_2CoMnO_6 thin films, Appl. Phys. Lett. 91 (2007) 202509 1-4. https://doi.org/10.1063/1.2814919

[46] R. N. Mahato, K. Sethupathia, V. Sankaranarayanan, Colossal magnetoresistance in the double perovskite oxide La_2CoMnO_6, J. Appl. Phys. 107 (2010) 09D714 1-3. https://doi.org/10.1088/0953-8984/23/49/496003

[47] J. K. Murthy, A. Venimadhav, Size dependent magnetic properties of double perovskite La_2CoMnO_6 nanoparticles, AIP Conference Proceedings. (2013) 1053-1054; https://doi.org/ 10.1063/1.4810596

[48] R. Galceran, C. Frontera, L. Balcells, J. Cisneros-Fernández, L. López-Mir, J. Roqueta, J. Santiso, N. Bagués, B. Bozzo, A. Pomar, F. Sandiumenge, and B. Martínez, Engineering the microstructure and magnetism of $La_2CoMnO_{6-\delta}$ thin films by tailoring oxygen stoichiometry, Appl. Phys. Lett. 105 (2014) 242401 1-3. https://doi.org/10.1063/1.4904410

Caption

Fig.1. X-ray diffraction profiles of experimental (. . .) and calculated patterns (—) for $La_2Ni_xCo_{1-x}MnO_6$ (x = 0.2, 0.25, 0.5, 0.75, 0.8). Star represents La_2MO_4 with M = Ni, Co, Mn (orthorhombic, space group Bbam).

Fig.2. The monoclinic structure with $P2_1/n$ space group of $La_2Ni_xCo_{1-x}MnO_6$ represented on Vesta program (K. Momma and F. Izumi (2011): J. Appl. Crystallogr., 44, 1272-1276).

Fig.3. Raman spectra of $La_2Ni_xCo_{1-x}MnO_6$ (x = 0.2, 0.25, 0.5, 0.75, 0.8) compounds.

Fig.4. Raman modes energy dependence with Nickel content of $La_2Ni_xCo_{1-x}MnO_6$.

Fig.5. FWHM versus the Nickel content of $La_2Ni_xCo_{1-x}MnO_6$ (x = 0.2, 0.25, 0.5, 0.75, 0.8) compounds.

Fig. 6. FT-IR spectra of $La_2Ni_xCo_{1-x}MnO_6$ (x = 0.2, 0.25, 0.5, 0.75, 0.8) compounds.

Fig.7. $(\alpha h\nu)^2$ versus photon energy ($h\nu$) of $La_2Ni_xCo_{1-x}MnO_6$ (x = 0.2, 0.25, 0.75, 0.8) compounds.

Fig.8.Results from the *M*agnetization-Temperature measurements for $La_2Ni_xCo_{1-x}MnO_6$ (x = 0.2, 0.25, 0.5, 0.75, 0.8) in the magnetic field of 50 Oe : thermal variation of ZFc-Fc molar susceptibility (χ_M) (a) and enlarged ZFc χ_M (b) in the temperature range of 2 - 300 K, derivative of ZFc χ_M versus temperature between 180 K and 300 K (c, the solid lines are eye guides) and inverted ZFc χ_M against temperature between 220 K and 300 K (d, the solid lines represent the data fitted by Curie-Weiss law).

Fig.9. Field dependent magnetization for $La_2Ni_xCo_{1-x}MnO_6$ (x = 0.2, 0.25, 0.5, 0.75, 0.8) at 5 K in the field range from -7 *T* to 7 *T* (a) and in the field range from -2 *T* to 2 *T* (b).

Fig.10.Field dependent magnetization for $La_2Ni_xCo_{1-x}MnO_6$ (x = 0.2, 0.25, 0.5, 0.75, 0.8) at 300 K in the field range from 0 to 7 *T*.

Fig.11.Thermal variation of the real and imaginary molar susceptibilities (χ' and χ'') for $La_2Ni_xCo_{1-x}MnO_6$ (x = 0.2, 0.25, 0.5, 0.75, 0.8) in an AC magnetic field of 3 Oe with three frequencies (50 Hz, 141.6 Hz and 400.6 Hz).

Table.1.Crystal parameters and details of the structure refinement for $La_2Ni_xCo_{1-x}MnO_6$ (x = 0.2, 0.25, 0.5, 0.75, 0.8).

Table.2. Bond distances (Å) for $La_2Ni_xCo_{1-x}MnO_6$ (x = 0.2, 0.25, 0.5, 0.75, 0.8).

Table.3. Results of The electron Probe Microanalysis (EPMA) analysis for the cation composition and concentration for $La_2Ni_xCo_{1-x}MnO_6$ (x = 0.2, 0.25, 0.5, 0.75, 0.8). The gap is the difference between experimental and theoretical concentration.

Table.4. Raman Lorentzian fitting parameters of the $La_2Ni_xCo_{1-x}MnO_6$ (x = 0.2, 0.25, 0.5, 0.75, 0.8) bands at RT.

Table.5. The band gap energy of $La_2Ni_xCo_{1-x}MnO_6$ (x = 0.2, 0.25, 0.75, 0.8) compounds and comparison to literature.

Table.6. Curie temperatures and Curie-Weiss parameters for $La_2Ni_xCo_{1-x}MnO_6$ (x = 0.2, 0.25, 0.5, 0.75, 0.8).

Table.7. Characteristics of the *M-H* loops at 5 K for $La_2Ni_xCo_{1-x}MnO_6$ (x = 0.2, 0.25, 0.5, 0.75, 0.8).

Table.8. Curie temperatures and cluster glass transition temperature determined by the out of phase molar susceptibility, χ''-*T* for $La_2Ni_xCo_{1-x}MnO_6$ (x =0.2, 0.25, 0.5, 0.75, 0.8).

Table.9. Relaxation time τ, activation energy E_a and Mydosh factor K determined by the Arrhenius law from the out of phase molar susceptibility, χ''-*T* for $La_2Ni_xCo_{1-x}MnO_6$ (x = 0.2, 0.25, 0.5, 0.75, 0.8).

.

	x = 0.2	x = 0.25	x = 0.5	x = 0.75	x = 0.8
a (A˚)	5.522(1)	5.518(4)	5.515(6)	5.522(2)	5.515 (8)
b (A˚)	5.482(4)	5.472(1)	5.469(6)	5.480(8)	5.467(2)
c (A˚)	7.768(7)	7.754(9)	7.752(7)	7.766(6)	7.750(1)
β°	90.08(2)	90.08(5)	90.07(8)	90.12(1)	90.04(4)
V $(A^{\circ})^3$	235.177(1)	234.176(3)	233.884(2)	235.039(2)	233.673(5)
La: x	0.0031(2)	0.0031(3)	0.0029(3)	0.0027(8)	0.0037(7)
y	0.5218(7)	0.5192(1)	0.5194(1)	0.5218(8)	0.5179(7)
z	0.2474(1)	0.250	0.2490(1)	0.2506(1)	0.2484(8)
B_{iso}	0.7321(9)	0.6823(4)	0.8497(3)	0.6933(1)	0.6589(5)
Mn: x y z	0 0 0	0 0 0	0 0 0	0 0 0	0 0 0
B_{iso}	0.5478(5)	0.9102(5)	0.4482(7)	1.4434(2)	2.5478(5)
Ni: x y z	0 0 0.5	0 0 0.5	0 0 0.5	0 0 0.5	0 0 0.5
B_{iso}	0.3007(9)	0.2312(4)	0.2063(3)	0.1083(8)	0.2314(3)
Occ	0.2000	0.25	0.5	0.75	0.8
Co: x y z	0 0 0.5	0 0 0.5	0 0 0.5	0 0 0.5	0 0 0.5
B_{iso}	0.3007(9)	0.2312(4)	0.2063(3)	0.1083(8)	0.2314 (3)
Occ	0.8000	0.75	0.5	0.25	0.2
O(1): x	-0.7786(1)	-0.7742(1)	-0.7752(2)	-0.7680(5)	-0.7733(9)
y	0.2641(9)	0.2431(3)	0.2641(9)	0.2618(9)	0.2430(8)
z	0.0419(6)	0.0510(1)	0.0420(2)	0.0406(5)	0.0518(2)
B_{iso}	1.5307(1)	1.1001(4)	0.9660(6)	1.0119(2)	0.1576(2)
O(2): x	-0.5644(1)	-0.5662(1)	-0.5690(1)	-0.5757(2)	-0.5697(6)
y	0.4943(5)	0.5001(5)	0.4921(1)	0.4979(6)	0.4933(7)
z	-0.2677(4)	-0.2620(1)	-0.2562(2)	-0.2571(4)	-0.2589(1)
B_{iso}	1.5307(1)	1.1012(4)	0.9660(6)	1.0192(9)	0.1576(2)
O(3): x	-0.2802(1)	-0.2710(2)	-0.2701(1)	-0.2698(1)	-0.2873(2)
y	0.1887(7)	0.2110(1)	0.1810(2)	0.1844(1)	0.1933(2)
z	-0.0132(2)	-0.0161(3)	-0.0159(3)	-0.0109(7)	-0.0102(7)
B_{iso}	1.5307(1)	1.1032(4)	0.9660(6)	1.0192(9)	0.1576(2)
R_B	3.140	3.729	6.010	4.348	3.355
R_F	4.719	5.562	7.300	7.049	6.028
R_P	13.2	22.8	14.3	23.6	14.3
R_{wp}	9.65	17.3	10.8	15.7	10.8
R_{exp}	5.77	13.41	6.24	14.30	6.35
χ	2.80	1.67	2.97	1.21	2.91

	x = 0.2	x = 0.25	x = 0.5	x =0.75	x=0.8
Ni/CoO_6 octahedra					
$Ni/Co–O_1 \times 2$	2.0362(0)	1.9947(7)	2.0178(2)	1.9990(1)	2.0996(1)
$Ni/Co–O_2 \times 2$	2.1099(1)	2.0388(6)	2.0208(7)	2.0396(1)	2.0432(1)
$Ni/Co–O_3 \times 2$	2.0964(0)	2.1495(9)	2.1609(3)	2.1483(0)	2.0478(0)
MnO_6 octahedra					
$Mn–O_1 \times 2$	1.9228(0)	1.9537(7)	1.9321(2)	1.9491(1)	1.8677(1)
$Mn–O_2 \times 2$	1.8399(1)	1.9342(6)	1.9306(7)	1.9329(1)	1.9083(1)
$Mn–O_3 \times 2$	1.8642(0)	1.8019(8)	1.7924(3)	1.8023(1)	1.9063(1)
LaO_6 octahedra					
$La-O_1$	2.4495(1)	2.5107(6)	2.4555(3)	2.5099(1)	2.4687(2)
$La-O_1$	2.5979(1)	2.5436(6)	2.5813(3)	2.5485(1)	2.4734(2)
$La-O_1$	2.8211(1)	2.8661(6)	2.8396(3)	2.8617(1)	2.9551(2)
$La-O_1$	3.1823(1)	3.1212(6)	3.1504(3)	3.1216(1)	3.1473(3)
$La-O_2$	2.4301(1)	2.3599(3)	2.3949(2)	2.3616(1)	2.3960(1)
$La-O_2$	3.1044(1)	3.1674(3)	3.1232(2)	3.1659(1)	3.1233(1)
$La-O_2$	2.8556(1)	2.8831(2)	2.8254(1)	2.8825(1)	2.8251(1)
$La-O_2$	2.6816(1)	2.6677(2)	2.7020(1)	2.6678(1)	2.7025(1)
$La-O_3$	3.1421(1)	3.1327(7)	3.1468(2)	3.1307(1)	3.1216(2)
$La-O_3$	2.5738(1)	2.5579(7)	2.5926(2)	2.5591(1)	2.5424(2)
$La-O_3$	2.8592(1)	2.8722(7)	2.8509(2)	2.8707(1)	2.8896(2)
$La-O_3$	2.4934(1)	2.5032(7)	2.4668(2)	2.5049(1)	2.4807(2)

a)$La_2Ni_{0.8}Co_{0.2}MnO_6$.

Atoms	La	Mn	Ni	Co	La/Mn	Co/Ni
Experimental	20.75334	9.63132	7.73818	1.8732	2.1547	0.2407
Theoretical	20.0000	10.0000	8.0000	2.000	2	0.25
The gap	0.75334	0.36868	0.26182	0.1268	0.1547	0.0093

b) $La_2Ni_{0.75}Co_{0.25}MnO_6$.

Atoms	La	Mn	Ni	Co	La/Mn	Co/Ni
Experimental	20.5958	10.8890	8.3350	2.5380	2.0568	0.3046
Theoretical	20.0000	10.0000	7.5000	2.5000	2	0.33
The gap	0.5958	0.889	0.835	0.038	0.0568	0.0254

c) $La_2Ni_{0.5}Co_{0.5}MnO_6$.

Atoms	La	Mn	Ni	Co	La/Mn	Co/Ni
Experimental	19.12193	9.53302	5.70478	4.80597	2.0586	0.842
Theoretical	20.0000	10.0000	5.000	5.000	2	1
The gap	0.87807	0.46698	0.70478	0.19403	0.058	0.158

d) $La_2Ni_{0.25}Co_{0.75}MnO_6$.

Atoms	La	Mn	Ni	Co	La/Mn	Co/Ni
Experimental	26.3448	11.16795	3.4892	7.205583	2.3720	2.0934
Theoretical	20.0000	10.0000	2.5000	7.5000	2	3.0000
The gap	6.3448	1.16795	0.9892	0.294417	0.3720	0.9066

e) $La_2Ni_{0.2}Co_{0.8}MnO_6$.

Atoms	La	Mn	Ni	Co	La/Mn	Co/Ni
Experimental	20.5053	9.6972	2.188675	7.60762	2.1145	3.4759
Theoretical	20.0000	10.0000	2.0000	8.0000	2	4.0000
The gap	0.5053	0.3028	0.188675	0. 60762	0.1145	0.5241

Samples	Peak 1 (cm^{-1})	FHWM 1(cm^{-1})	Peak 2 (cm^{-1})	FHWM 2 (cm^{-1})
$La_2Ni_{0.80}Co_{0.20}MnO_6$	522	114	663	48
$La_2Ni_{0.75}Co_{0.25}MnO_6$	523	46	667	41
$La_2Ni_{0.50}Co_{0.50}MnO_6$	518	63	658	43
$La_2Ni_{0.25}Co_{0.75}MnO_6$	516	141	647	55
$La_2Ni_{0.20}Co_{0.8\ 0}MnO_6$	508	75	651	37

Theoretical formula	experimental formula	band gap energy (eV)	Ref
La_2NiMnO_6	La_2NiMnO_6	1.2	[30]
$La_2Ni_{0.8}Co_{0.2}MnO_6$	$La_{2.07}Ni_{0.77}Co_{0.18}Mn_{0.96}O_6$	1. 66(2)	This work
$La_2Ni_{0.75}Co_{0.25}MnO_6$	$La_{2,05}\,Ni_{0.83}\,Co_{0,25}\,Mn_{1.08}O_6$	1. 65(1)	This work
$La_2Ni_{0.25}Co_{0.75}MnO_6$	$La_{2.6}\,Ni_{0.34}Co_{0.72}Mn_{1.1}O_6$	1.75(1)	This work
$La_2Ni_{0.2}Co_{0.8}\,MnO_6$	$La_{2.05}Ni_{0.21}Co_{0.76}Mn_{0.96}O_6$	1. 62(2)	This work
La_2CoMnO_6	La_2CoMnO_6	1.93	[29]

Sample	T_c (ZFC-FC)		Reference	Curie-Weiss constants			Reference
	T_{c1} (K)	T_{c2} (K)		C_{Curie} ($cm^3.K.mol^{-1}$)	Θ (K)	Effective moment (μ_B)	
x=0	210		[33]			7.34	[33]
x = 0.20	232.0	200.0	This work	6.743	236.92	7.52	This work
x = 0.25	238.0	200.0	This work	7.790	246.56	7.483	This work
x = 0.50	243.0	208.0	This work	5.927	250.24	6.85	This work
x = 0.75	255.0		This work	6.857	261.58	6.12	This work
x = 0.80	260.0		This work	7.106	266.20	7.49	This work
x = 1	280		[35]			5.54	[35]

Double Perovskite	Spin-only M_{S0} ($\mu_{B/f.u.}$)	Characteristics of hysteresis cycle at 5 K			
		M_{S0} ($\mu_{B/f.u.}$)	Order degree (%)	H_C (KOe)	M_r ($\mu_{B/f.u.}$)
x =0.20	5.81	5.14	88.47	3.5	2.56
x =0.25	5.77	4.50	77.99	2.0	2.01
x =0.50	5.52	4.90	88.73	2.0	2.30
x =0.75	5.27	5.09	96.58	1.0	1.97
x =0.80	5.22	5.41	100.00	0.8	1.96

Double perovskite 's composition	FM transition temperature (K)		Frequency dependent transition temperatures of cluster glass (K)		
	T_{C1ac}	T_{C2ac}	T_{f1} (50 Hz)	T_{f2} (141.6 Hz)	T_{f3} (400.6 Hz)
x = 0.20	230.0	195.0	75.0	85.0	95
x = 0.25	236.0	195.0	90.0	100.0	110
x = 0.50	239.0	203.0	70.0	75.0	80
x = 0.75	250.0		65.0	70.0	75
x = 0.80	255.0		70.0	80.0	90

Double perovskite 's composition	τ0 (s)	Ea (cm^{-1})	K
x = 0.20	1.759 ×10-7	512.872	0.260
x = 0.25	3.659×10-8	713.529	0.221
x = 0.50	1.963×10-10	808.713	0.147
x = 0.75	5.573×10-10	703.860	0.158
x = 0.80	2.974×10-7	453.219	0.277

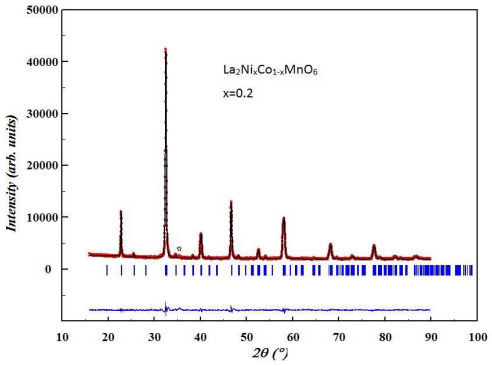
La2NixCo1-xMnO6
x=0.2
Intensity (arb. units)
2θ (°)

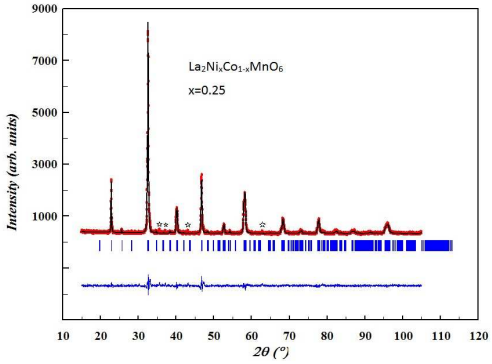
La2NixCo1-xMnO6
x=0.25
Intensity (arb. units)
2θ (°)

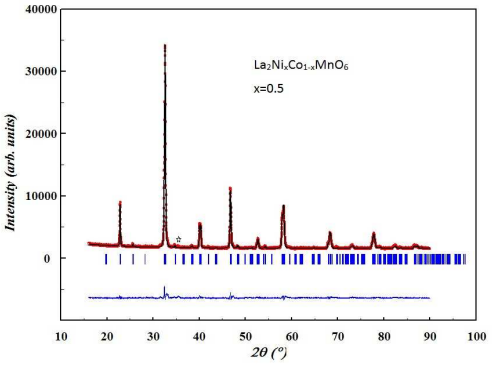
La2NixCo1-xMnO6
x=0.5
Intensity (arb. units)
2θ (°)

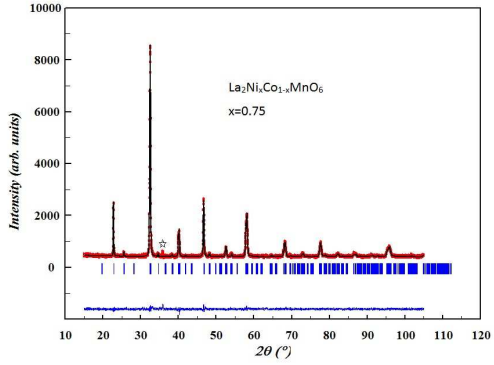
La2NixCo1-xMnO6
x=0.75
Intensity (arb. units)
2θ (°)

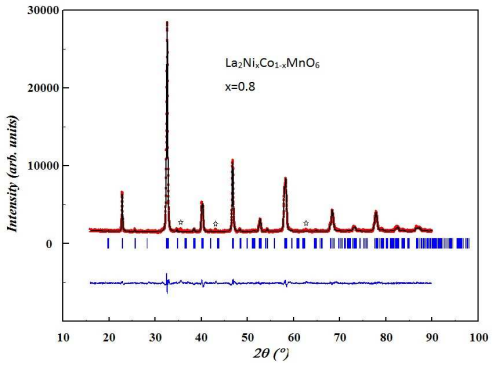
La2NixCo1-xMnO6
x=0.8
Intensity (arb. units)
2θ (°)

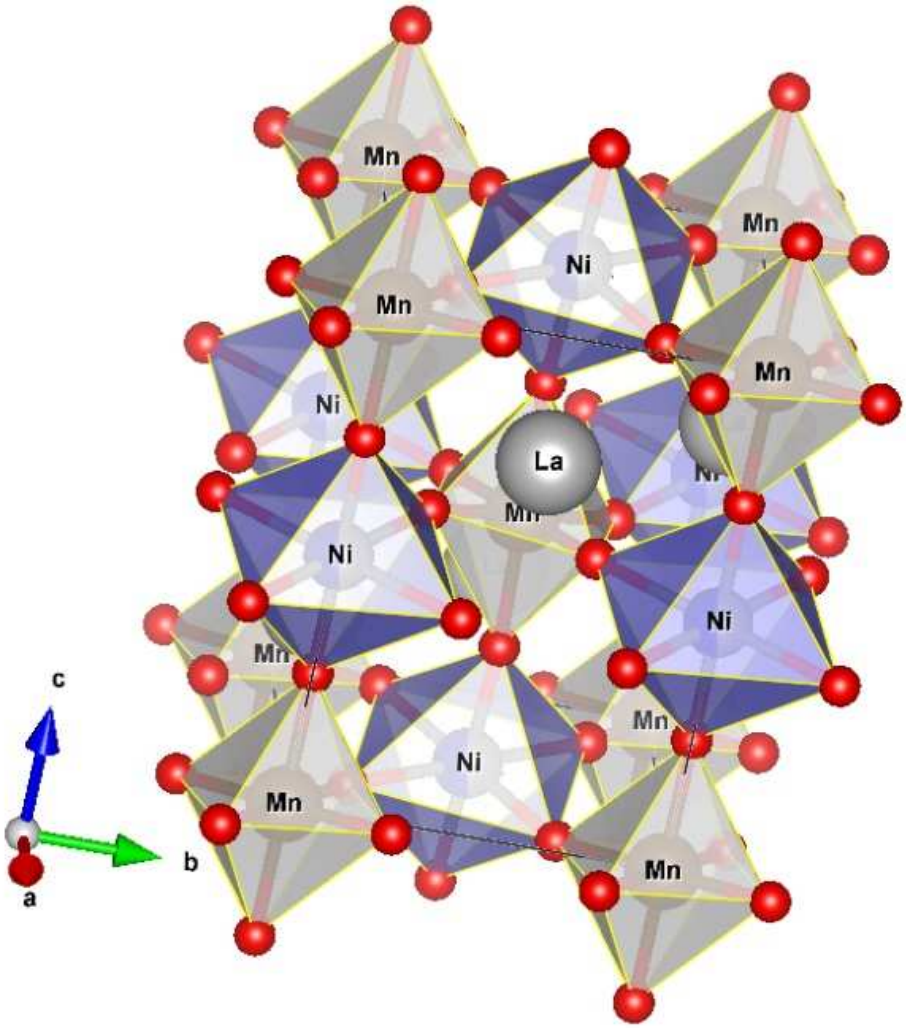

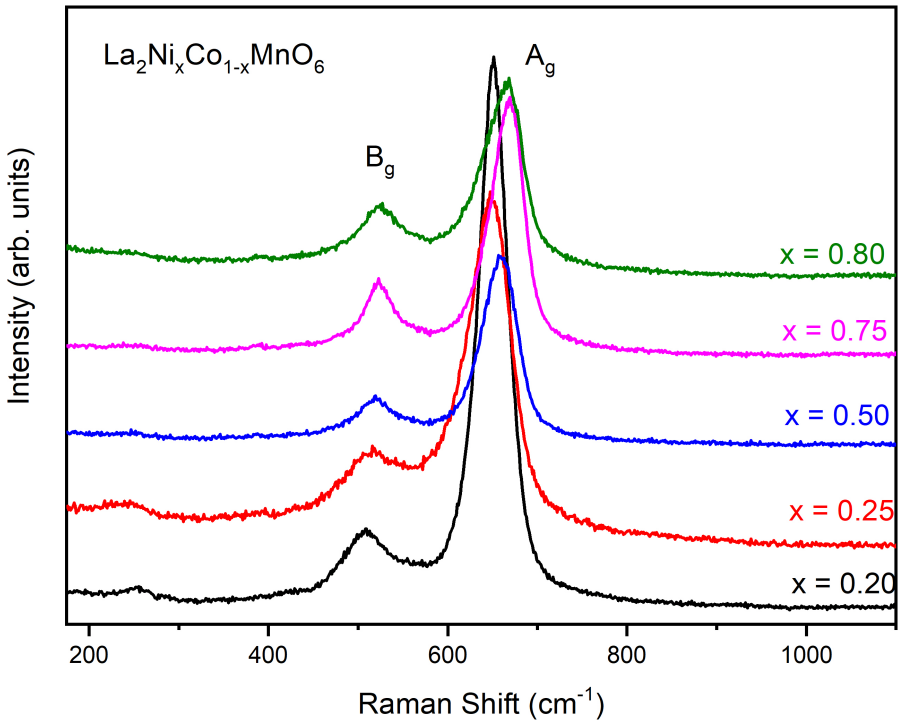

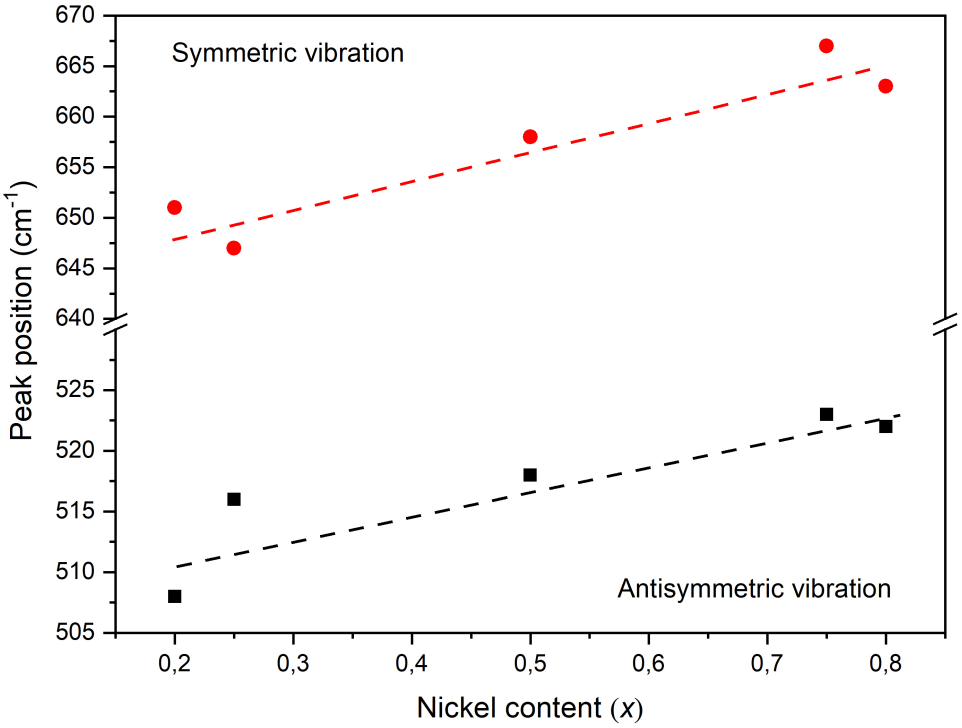

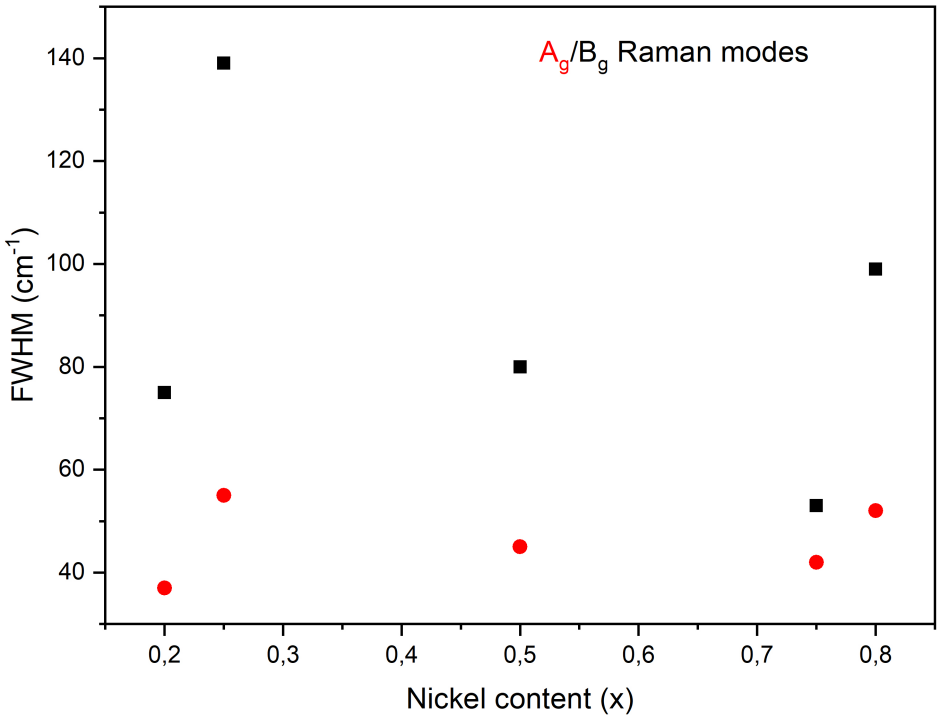

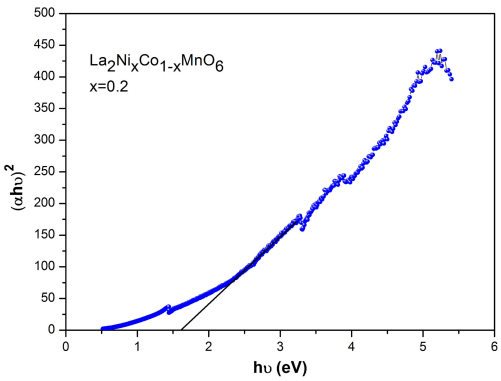
La2NixCo1-xMnO6
x=0.2
(αhυ)2
hυ (eV)

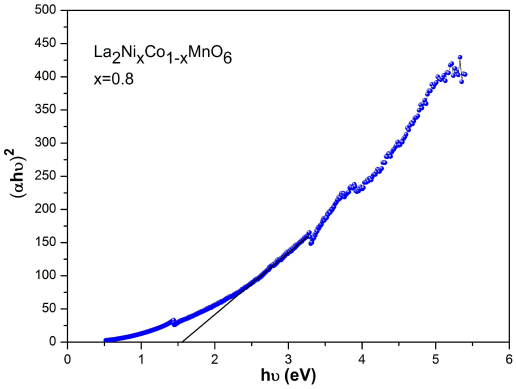
La2NixCo1-xMnO6
x=0.8
(αhυ)2
hυ (eV)

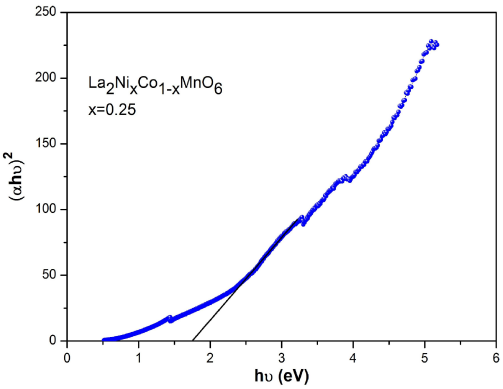
La2NixCo1-xMnO6
x=0.25
(αhυ)2
hυ (eV)

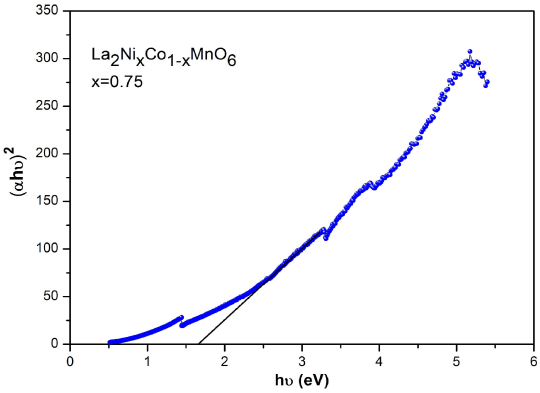
La2NixCo1-xMnO6
x=0.75
(αhυ)2
hυ (eV)

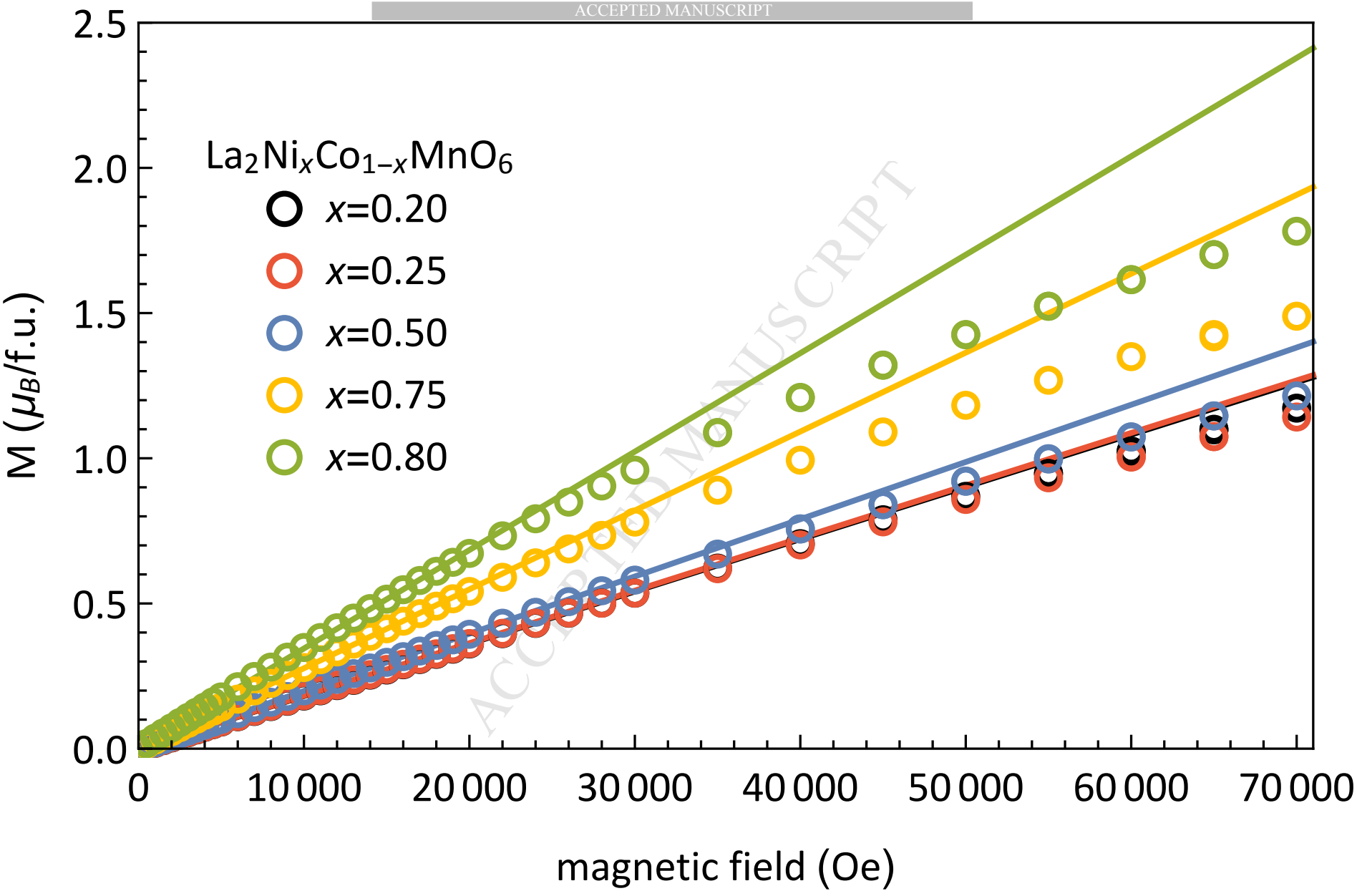

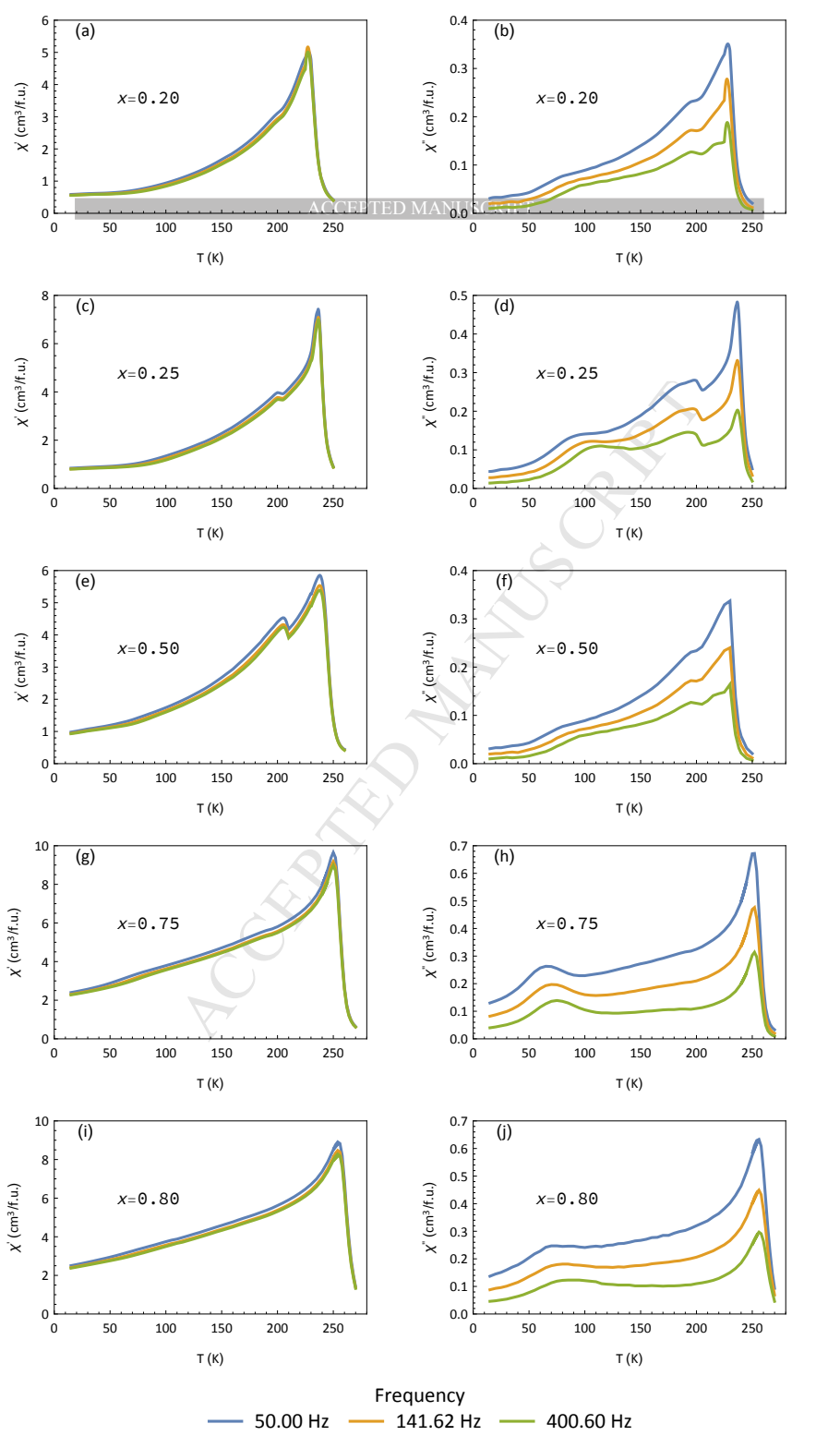

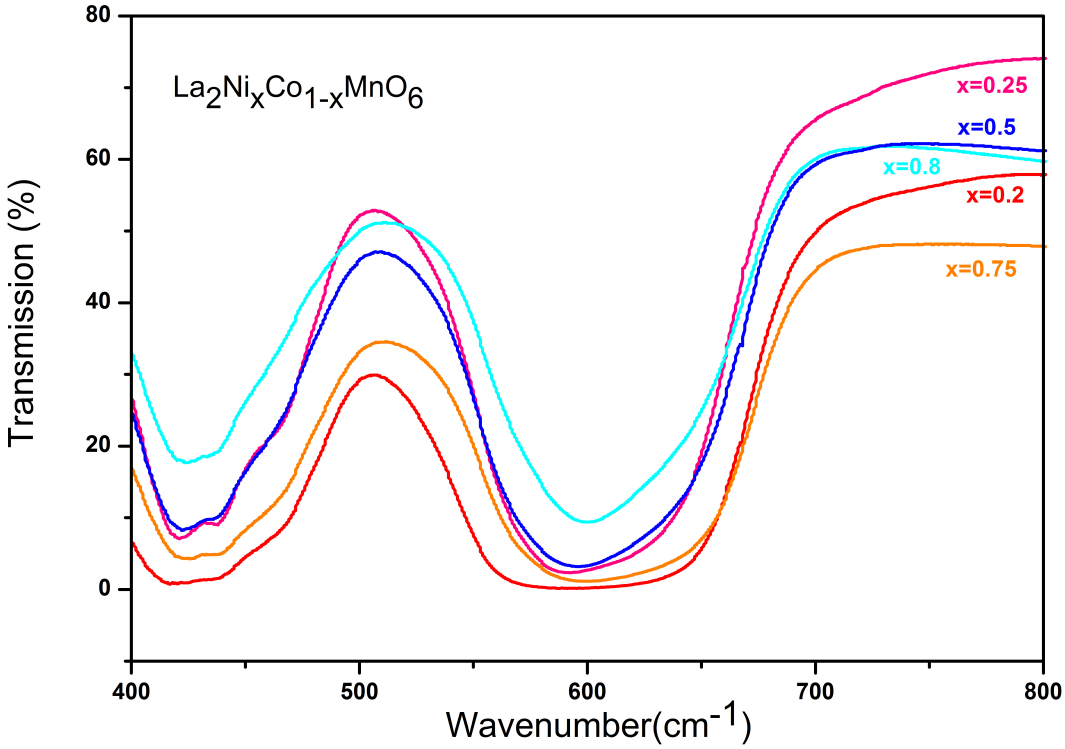

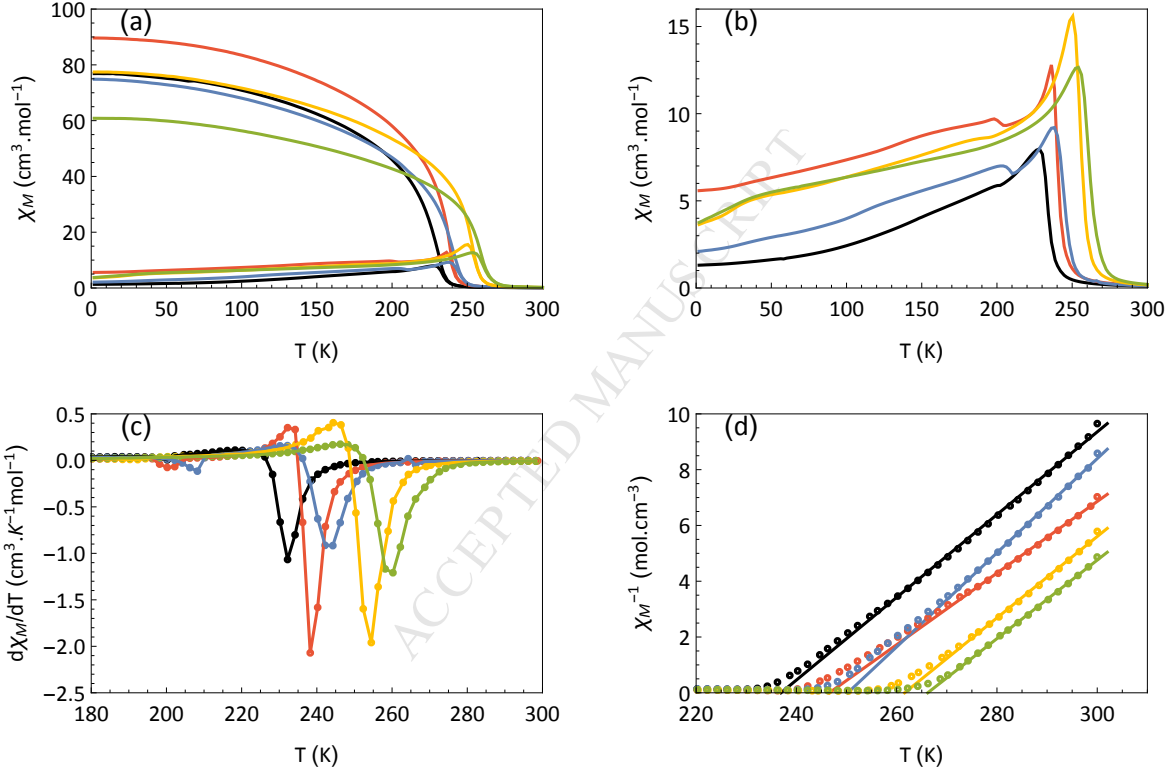

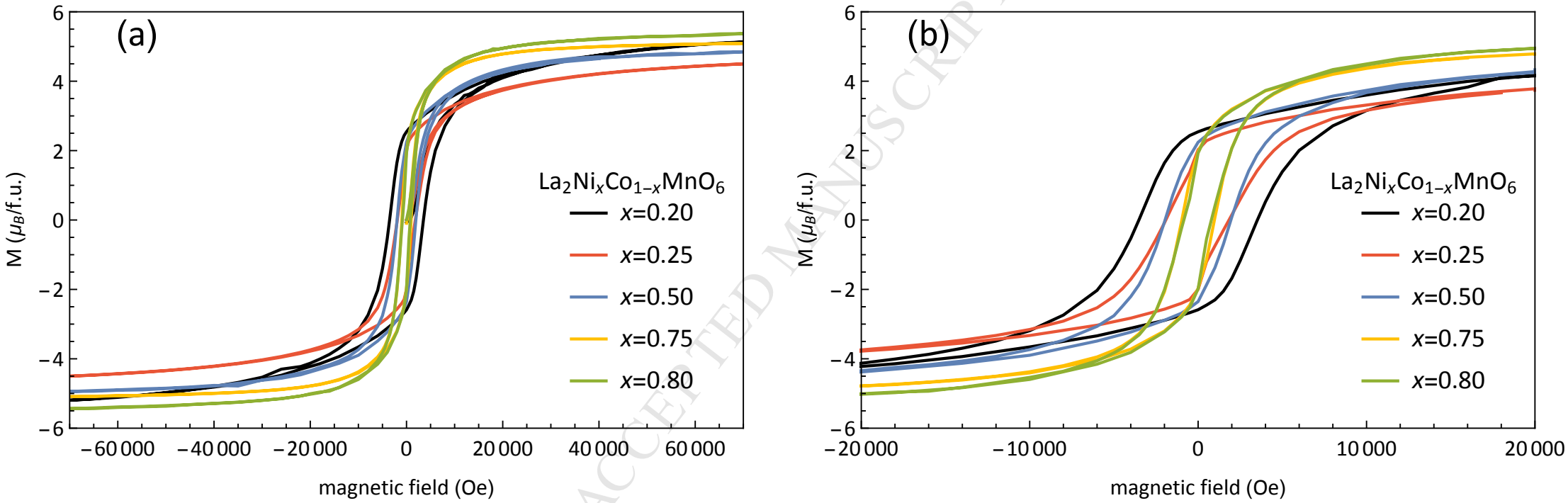

Highlights

Highlights

- The effect of cation disorder on magnetic properties of double perovskites $La_2Ni_xCo_{1-x}MnO_6$
- Paramagnetic to ferromagnetic (PM-FM) transition
- Existence of super-paramagnetic mono-domains
- Revealing spin glass transition analog.
- Double-perovskite La_2NiMnO_6 is a single material platform with multiple functions